Summer 2017

Ti-Fe intermetallics analysis and control in joining titanium alloy and stainless steel by laser metal deposition

Wei Li

Recommended Citation

Li, Wei, "Ti-Fe intermetallics analysis and control in joining titanium alloy and stainless steel by laser metal deposition" (2017). *Masters Theses*. 7856.
https://scholarsmine.mst.edu/masters_theses/7856

TI-FE INTERMETALLICS ANALYSIS AND CONTROL IN JOINING TITANIUM ALLOY AND STAINLESS STEEL BY LASER METAL DEPOSITION

By

WEI LI

A THESIS

Presented to the Faculty of the Graduate School of the

MISSOURI UNIVERSITY OF SCIENCE AND TECHNOLOGY

In Partial Fulfillment of the Requirements for the Degree

MASTER OF SCIENCE IN MANUFACTURING ENGINEERING

2017

Approved by

Dr. Frank Liou, Advisor

Dr. Joseph Newkirk

Dr. Heng Pan

ABSTRACT

Direct fusion joining titanium alloy and stainless steel can cause brittle Ti-Fe intermetallics which compromise the mechanical properties of diffusion bonds between titanium alloys and stainless steel. Therefore, filler metals are required as transition layers. In this research, stainless steel metallic powder was directly deposited on the titanium alloy substrate by laser beam, the Ti-Fe intermetallic phases formed in this process were investigated through analyzing fracture morphology, phase identification, and Vickers Hardness Number (VHN). After that, Laser Metal Deposition (LMD) was applied to explore a new fabricating process to join Ti6Al4V and SS316. A transition composition route was introduced (Ti6Al4V→V→Cr→Fe→SS316) to avoid the intermetallic phase between Ti6Al4V and SS316. A thin wall sample was fabricated via LMD following the transition composition route. X-ray Diffraction (XRD) tests were conducted. The results demonstrate that the generation of intermetallic phases is effectively avoided following the composition route. Microstructure characterization and composition distribution analysis were performed via Scanning Electron Microscope (SEM) and Energy Dispersive Spectrometry (EDS). The SEM results indicated that rapid solidification results in the elongated microstructure. The EDS result can reflect the transition composition route design. Besides, the diffusions of metals are detected in the EDS results. Vickers hardness test was executed to observe the VHN distribution from Ti6Al4V to SS316. Vickers hardness result showed that there was no significant formation of intermetallic phases. Comparing with directly depositing SS316 on Ti6Al4V, the usage of the new transition route can eliminate the Ti-Fe intermetallics effectively.

ACKNOWLEDGMENTS

I would like to express my sincere gratitude to my advisor Dr. Frank Liou for the opportunity to work under him in LAMP lab. His financial support, guidance and remarks were vital throughout my graduate studies and achieving success in my work. I would like to thank the members of my thesis committee Dr. Joseph Newkirk, and Dr Heng Pan for their assistance and advice on my research work.

I would like to express my gratitude towards Karen Taminger and William J. Seufzer from NASA for their timely advice and help in supporting this project. I thank all members of LAMP lab for their supports, especially Sreekar Karnati, Jingwei Zhang, Yunlu Zhang, Xueyang Chen, Lei Yan, Caitlin Kriewall, etc.

Finally, thanking my family members for their support and love.

TABLE OF CONTENTS

Page

SECTION

LIST OF ILLUSTRATIONS

LIST OF TABLES

1. INTRODUCTION

1.1. BACKGROUND

Titanium and Ti series alloys have addressed a lot of concerns because they are considered some of the best engineering materials in the aerospace, nuclear, and chemical industries. They are known for their particular mechanical and metallurgical properties such as light weight, high strength-to-weight ratio, and superior heat resistance. In the aerospace industry, Ti alloy is a significant material of choice for requiring a lightweight surface coupled with strong heat resistance. For example, Ti alloy in an atmosphere of 500 ℃ maintains very good strength and stability. Several kinds of aircraft, such as missiles and rockets, fly at super high speed so their engine and surface temperatures are quite high. In this working situation, the Ti alloy is more appropriate than other metal alloys with relatively weak heat resistances.

In order to combine good mechanical and metallurgical properties of titanium alloys, and either good formability or economic prices of other alloys, there is an upsurge of interest to join Ti alloys with dissimilar structural steels or stainless steels. It is well known that stainless steel is good for weldability and is much more economic than costly Ti alloys. Unfortunately, the traditional heat fusion welding has not yet been technically capable of joining Ti alloy with stainless steel because of a metallurgical incompatibility between them [1]. Direct heat fusion welding of Ti alloy and stainless steel can result in the formation of a variety of intermetallic compounds such as TiFe, TiFe2, and so on. These intermetallic compounds are brittle and can embrittle the joint [2]. In addition, residual stress and excessive generation of strains at the interface may arise from the thermal expansion difference of dissimilar alloys. All of the above negative factors ultimately result in corrosion fatigue failure during usage and service, even failure may happen in the joining process.

1.2. LITERATURE REVIEW

Thus, many previous researchers performed studies to find an appropriate joining method from existing technologies such as heat fusion welding, diffusion welding, explosive welding, laser metal powder deposition, electron beam deposition, etc. They also sought the proper metal or alloy to insert as an interlayer in order to eliminate or relieve the influence of intermetallic compounds, or accommodate the residual stress concentration. Evren and Nizamettin [3] joined Ti and low-carbon steel plates through diffusion bonding using an Ag interlayer. The work showed that the Vickers hardness values on both sides of the interlayer decreased gradually as the distance from the joint increased. This indicated that the intermetallic phase of Ti and Fe was controlled in the Ag-rich area. Wang and Zhang [4] applied electron beam welding to join Ti-15-3 alloy and SS304 stainless steel using a Cu sheet as the interlayer. These two alloys were welded but intermetallics were found. Elrefaey and Tillmann [5] also used a Cu-based alloy as an interlayer to bond Ti and steel, by using diffusion bonding. These two dissimilar alloys were joined together, but must be operated at a diffusion temperature of more than 800 ℃. In addition, Kundu and Sam [6] analyzed interfacial reactions and strength properties in diffusion bonding Ti alloy and micro-duplex stain-less steel using a Ni alloy as intermediate material. Kundu and Chatterjee [7] investigated the interface microstructure and strength properties of diffusion bounded joints of Ti and 18Cr-8Ni stainless steel using a 120 μm thick Al interlayer as transition material. Some researchers also considered using multi-interlayers as the transition material. Peng, Jinglong, and Jiangtao [2] conducted diffusion bonding processing to join Ti alloy to austenitic stainless steel. They used the Nb→Cu→Ni transition structure as the multi-interlayer. Lee, Lee, and Choi [8] chose V→Cr→Ni as the multi-interlayer to join Ti alloy and stainless steel using diffusion bonding processing.

Based on the above research summaries, the frequently used interlayer metals are Cu, Ni, Ag, Al, Nb, etc. The selection of the interlayer material depends on its metallurgical properties with Ti and Fe, especially if the interlayer material can form the intermetallic phase with Ti and Fe in the cooling process after experiencing high-temperature solution annealing. However, although interlayer metals were used in the above researches, Ti-Fe or other Ti-related intermetallics were always found more or less between titanium alloy and stainless steel. In another word, the intermetallics were not completely eliminated based on the above interlayer design.

1.3. LASER METAL DEPOSITION PROCESS

Laser Metal Deposition (LMD) is an advanced additive manufacturing technology which can directly produce fully dense, functional metal parts. In its operation, a laser beam is focused on a metallic substrate to create a melt pool. A powder stream is continuously conveyed into the melt pool by the powder delivery system. Because of the advantages of high energy density, precise and flexible heating position, and laser beam radius, LMD was the most frequently used fusion welding method to join dissimilar metals. In this method, only a small heat-affected zone can be produced, and the process can be completed in a short time period [9]. The substrate is attached to a computer numerical control (CNC) multi-axis system. By moving the substrate according to a desired route pattern, a 2D layer can be deposited. Then, a 3D object can be formed through building successive layers on top of one another.

With the purpose of finding an effective interlayer or material transition route between titanium alloy and stainless steel for LMD, in the present study, stainless steel metallic powder was directly deposited on the titanium alloy substrate by laser beam first. The Ti-Fe intermetallic phases formed in this process were investigated through analyzing fracture morphology, phase identification, and Vickers Hardness Number (VHN). Then, LMD was applied to explore a new fusion fabricating process to produce the continuously graded material joining Ti6Al4V and SS316. Since cracking occurred when SS316 was directly deposited on Ti6Al4V and contributed to a large amount of intermetallic phase, a new transition composition route was designed to prevent the formation of the intermetallic phase. A thin wall sample was fabricated by LMD following the transition composition route. Microstructure characterization and transition composition distribution analysis was performed by the Scanning Electron Microscope (SEM) and Energy Dispersive Spectrometry (EDS) techniques. X-ray Diffraction (XRD) tests were conducted in order to identify the phases generated in the fabrication. Finally, Vickers hardness test was executed to observe the VHN distribution from Ti6Al4V to SS316. By comparing with directly depositing SS316 on Ti6Al4V, the new transition route was evaluated.

2. TI-FE INTERMETALLICS IN LASER DEPOSITING SS316 ON TI6AL4V

2.1. SAMPLE FABRICATION

Laser direct deposition to join titanium alloy and stainless steel is hindered by the formation of interfacial intermetallics caused by metallurgical reactions. Ti-Fe intermetallics are the main obstructive. To investigate the Ti-Fe intermetallics in the process of laser deposition, SS316 metallic powder was deposited on Ti6Al4V substrate directly by fiber laser (Figure 2.1.a), then analyzed fracture morphology (Figure 2.1.b), phase identification (Figure 2.2), and Vickers Hardness Number (Figure 2.3). The LMD operating parameters are shown in Table 2.1.

Table 2.1. The operating parameters in depositing SS316 on Ti6Al4V by LMD

Laser	Fiber laser CW
Output power (W)	550
Beam diameter (mm)	2
Scan speed (mm/min)	200
Shielding gas	Argon
Powder feed rate (g/min)	7.2

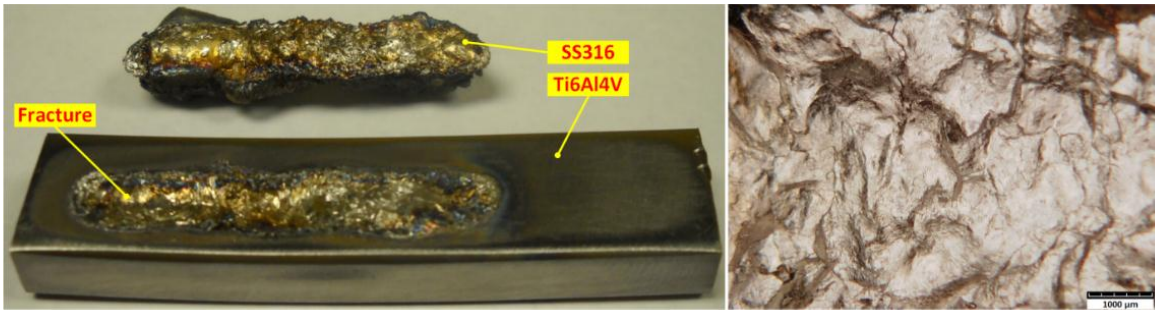

(a). SS316 layer fell off from Ti6Al4V substrate; (b).Fracture morphology

Figure 2.1. Direct deposition of SS316 on Ti6Al4V substrate.

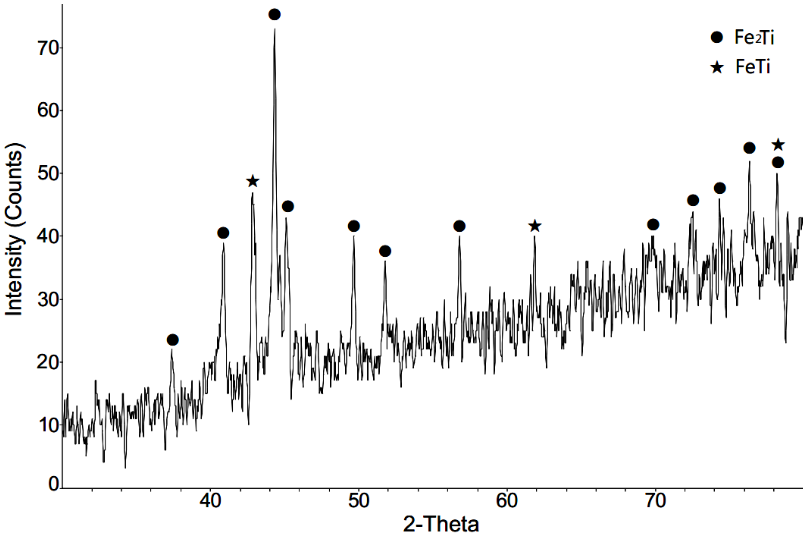

Figure 2.2. XRD pattern on the fracture area.

2.2. FRACTURE MORPHOLOGY AND PHASE IDENTIFICATION

As shown in Figure 2.1.a, SS316 metallic powder was deposited on Ti6Al4V substrate by fiber laser. In this process, the stainless steel layer directly fell off from titanium substrate coupled with clear cracking sound. The morphology in the fracture area is shown in Figure 2.1.b. It can be clearly observed the fracture morphology is relative smooth. By observing this fracture morphology, the fracture mechanism is classic cleavage fracture, which is caused by disruption surface's separating along some crystal plane. Cleavage fracture always happens in body-centered cubic (BCC) and hexagonal close-packed (HCP) metal or alloy. Its crack-evolution is very fast so that resulting in metallic component's disastrous collapse. This phenomenon indicates that the formed phase in fracture area is very hard and brittle, and almost without any plasticity. XRD test was per-formed on the fracture area to identify the formed phase. The XRD pattern in Figure.2.2 indicates that main inter-metallic phases are Fe2Ti and FeTi. The brittleness and hardness of these two caused the direct fracture and clear cracking sound under thermal stress and excessive generation of strains at the interface arising from the thermal expansion difference of titanium and stainless steel alloys.

2.3. VICKERS HARDNESS NUMBER DISTRIBUTION NEAR CRACK

Vickers hardness tests were conducted from Ti6Al4V side to SS316 side. The result is described in Figure. 2.3. The VHN near crack region is much larger than the base alloys on both sides. It can demonstrate that the compounds near crack region have poor plasticity. The crack can generate just under the action of pretty small thermal stress. From the VHN distribution in Figure.2.3, it turns out that VHN keeps approximately in Ti6Al4V substrate then starts to increase when close to the crack region, and reaches the maximum value of 1130 VHN. The perforative crack happened at this location. The VHN distribution in Figure. 2.3 illustrates that the formation of intermetallic phases is the primary cause for the failure when directly laser depositing stainless steel powder on titanium alloy substrate.

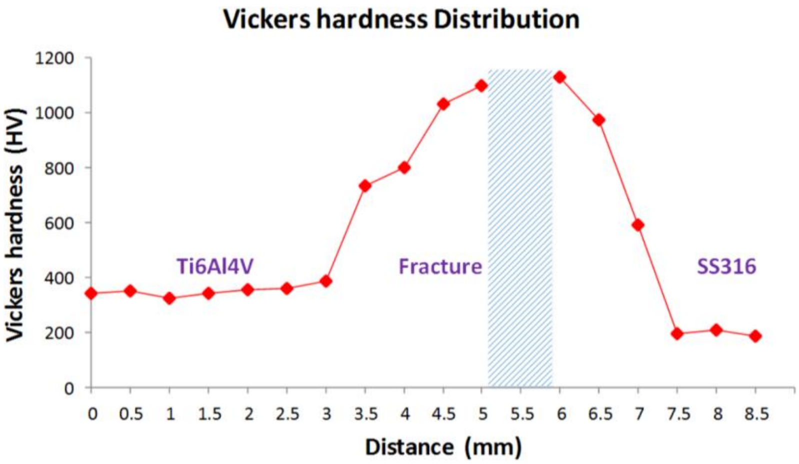

Figure 2.3. Vickers hardness number distribution near crack.

3. DEPOSITING TI6AL4V TO SS316 WITH NOVEL TRANSITION ROUTE

3.1. TRANSITION ROUTE DESIGN

Based on previous research experiences, it was impossible to join Ti6Al4V and SS316 directly because of the large amount of Ti-based intermetallic phases. The critical solution was to find an interlayer metal as a transition composition to prevent the formation of an intermetallic phase. However, there is no element that has sufficient solubility with both Ti and Fe. In other words, the elements that are highly soluble with Ti will generate intermetallic phases with Fe because of their limited solubility with Fe and vice versa. It is reasonably concluded that only one insert metal could be insufficient to avoid the intermetallic phase in the joining of Ti6Al4V and SS316 [8]. Therefore, multi-interlayer metals are necessary to fundamentally address the intermetallic phase and brittleness.

Vanadium (V) was first considered as a suitable transition metal since V exhibits an excellent solubility with Ti as shown in the binary alloy phase diagram for the Ti-V system in Figure. 3.1(a). The beta-phase Ti forms a complete range of solid solutions with V, whereas the behavior of alpha-phase Ti is more limited in this respect. These promising properties of V as a transition metal are further enhanced by thermal expansion coefficients which form a ratio (Ti:V) of 8.5:8.3 [8]. As shown in the binary alloy phase diagram for the V-Cr system in Figure. 3.1(b), V and Chromium (Cr) exhibit unlimited mutual solid solubility across the entire system beneath the solidus. So Cr is a candidate metal as an adjacent transition material.

Since Cr has been selected as the candidate metal, next question is what material is appropriate to fill between Cr and SS316. In any case, Fe is the most compatible with SS316. In the Fe-Cr binary alloy system, a pure sigma phase exists between 472 ℃ and 830 ℃ if the mass percentage of Cr is greater than 42.7 wt% and less than approximately 48.2 wt%, as shown in the binary alloy phase diagram for the Fe-Cr system in Figure. 3.1(c). It is also obvious that there is no sigma phase precipitation beneath 472 ℃ and close to room temperature. Literature from previous studies [10, 11], has reported this type of brittle intermetallic sigma phase that is always observed in various series of

Duplex stainless steels. The sigma phase is often precipitated under an elevated temperature environment, such as casting, rolling, welding, forging, and aging [12].

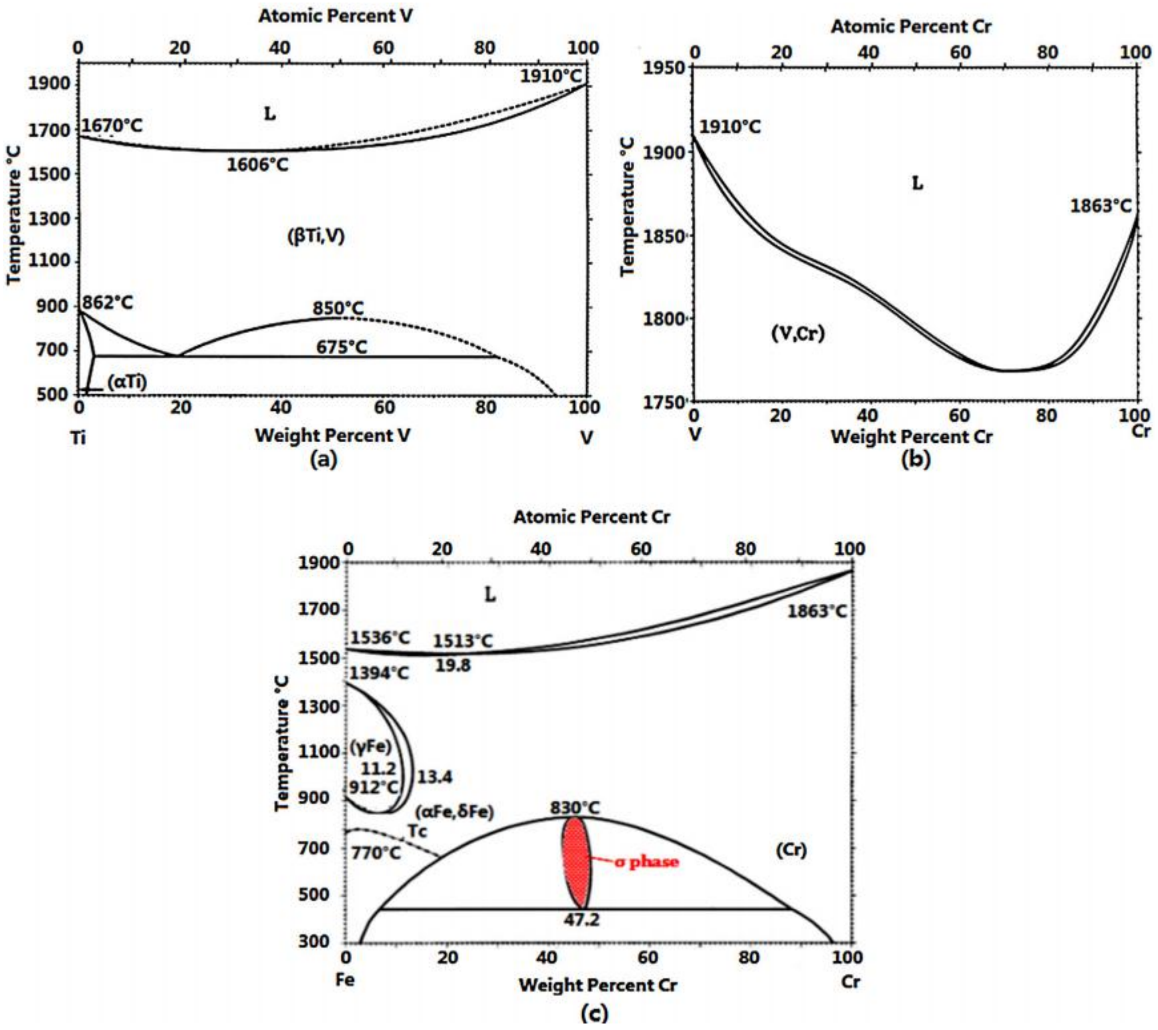

Figure 3.1. Binary alloy phase diagram of Ti-V (a), V-Cr (b), and Fe-Cr (c) [13]

After reviewing previous research and experiment results, the properties of the sigma phase in the Fe-Cr binary alloy system can be summarized as follows. Sigma phase exhibits a tetragonal structure [14]. It is a brittle phase and can decrease the toughness of the system [10]. Sigma phase forms in the cooling process from high temperatures, which is a metaphase in Fe-Cr binary system. To avoid the formation of more than 1% sigma phase, the cooling rate must exceed 0.23 ℃/s [14].

Investigation of the Fe-Cr phase diagram reveals that in the cooling process, if the temperature is lower than around 472 ℃, the dominant phases are the stable solid solutions, instead of the intermetallic sigma phase. Moreover, the cooling rate is an important factor in controlling the sigma phase’s formation, since large cooling rates can greatly bypass the dangerous temperature range from 472 ℃ to 830 ℃, and reduce the probability of the sigma phase formation. The previous researchers observed the cooling rate in LMD [15]. The minimum cooling rate value was guaranteed to be larger than 1 ℃/s under the laser processing parameters in Table 3.3. Based on the above analysis, in order to effectively avoid the Ti-based intermetallics, one new transition composition route: Ti6Al4V→V→Cr→Fe→SS316, was determined. Then laser metal powder deposition experiment was conducted following this composition route.

3.2. EXPERIMENT PROCEDURE

3.2.1. Materials and Preparation. Materials used in this experiment were Ti6Al4V, SS316, V, Cr, and Fe. Ti6Al4V and SS316 were regarded as the target materials since the objective was to join these two materials. V, Cr, and Fe were used as filler composition that transitions from Ti6Al4V to SS316 successively. The chemical compositions of Ti6Al4V and SS316 are given in Table 3.1. The V, Cr, Fe, and SS316 are in the form of pure powder. The powder characterization was introduced in next section. The Ti6Al4V is prepared in the form of a 2 ×0.5 ×0.25 in bar. In the process of laser metal powder deposition, the Ti6Al4V bar was used as a substrate. V, Cr, Fe, and SS316 powder were deposited on the top surface of the Ti6Al4V bar successively. The composition route is shown in Figure. 3.2.

Table 3.1. Chemical composition of the target materials (wt%)

Materials	C	Mn	Si	P	H	S	Cr	Al	V	Mo	O	Ni	N	Fe	Ti
Ti6Al4V	0.08	-	-	-	0.025	-	-	6.76	4.5	-	0.2	-	-	0.25	Balance
SS316	0.03	2	0.75	0.045	-	0.03	18	-	-	3	-	14	0.1	Balance	-

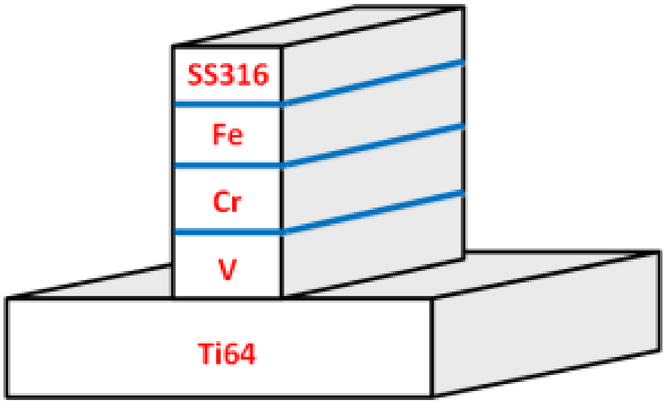

Figure 3.2. Composition route from Ti6Al4V to SS316.

The powders used in this research were characterized to analyze particle shape and size distribution. The quality of deposits could be potentially correlated with particle size and shape, so it is necessary to observe and analyze the size distribution and particle shape to explain some findings in the deposits. Microscope images (Figure 3.3) were taken by SEM equipment (Hitachi S4700). The particles size distributions for all the four types of powder were displayed by the sieve analysis in Table 3.2.

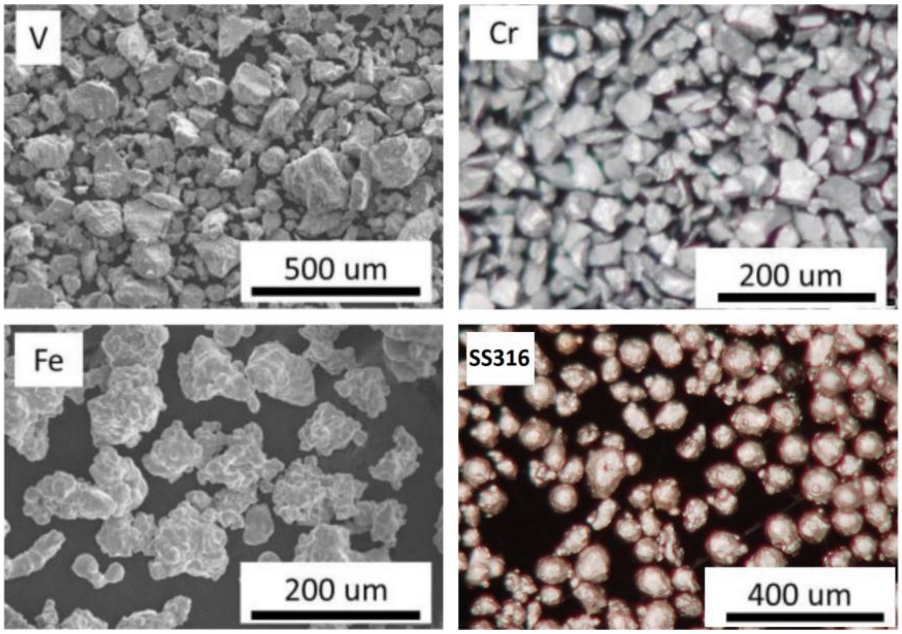

Figure 3.3. SEM Micrograph of the four types of powder.

Figure.3.3 shows four SEM micrographs acquired from the four types of powder. The V particles present irregular shape. The Cr particles present a very angular shape. The Fe particles have irregular shapes. SS316 powder particles have a mostly spherical shape when compared to the Fe and Cr powder particles.

Table 3.2. Sieve analysis of V, Cr, Fe, and SS316 powder

Sieve type	70 mesh	100 mesh	120 mesh	140 mesh	200 mesh	325 mesh
Size (μm)	>212	150-212	125-150	106-125	75-106	45-75
Percentage (%).V	1.3	4.0	8.4	23.7	27.4	35.2
Percentage (%).Cr	0.0	0.6	5.9	9.3	12.7	71.5
Percentage (%).Fe	3.1	9.2	22.4	35.1	21.8	8.4
Percentage (%).SS316	0.0	0.3	3.8	9.0	48.2	38.7

3.2.2. Laser Metal Powder Deposition Set-up. In this study, the laser metal powder deposition set-up consists of the following units: a laser system which provides the heat source, a powder feeding system with a ceramic nozzle, and a CNC table.

- For the laser heat source, a continuous wave (CW) fiber laser system with a 1.064 μm wavelength was used. The laser system can provide at most 1000 W laser output power. The laser energy intensity was in accordance with Gaussian distribution. The optics in the laser beam delivery system provides a beam diameter of 2 mm in this experiment.
- The powder feeding system consists of a powder container and a gas carrying pipeline system. In this study, several different kinds of metal powder were changed using the powder container. Then, inert Ar was used as a carrying gas to move the powder from the powder container through the pipeline system. The flowing Ar carrying the metal powder was sprayed through an Al_2O_3 ceramic nozzle so that the metal powder reached the melt pool area.
- The CNC table was used to generate the displacement of the substrate in a horizontal direction and the displacement of the laser beam delivery system in a vertical direction so that the laser deposition path could be created.

3.2.3. Experimental Procedure. The laser metal powder deposition procedure is depicted in Figure. 3.4. A 3D thin wall sample was fabricated layer by layer with different metal powders deposited on the surface of a moving Ti6Al4V substrate. In order to observe the property of the different powders at different layers conveniently, the sample was fabricated in the form of a thin wall structure. The laser processing parameters are explained in Table 3.3. The fiber laser was set as the CW mode. One point should be noted that the laser output power varied in the range of 550 W to 1 kW. Since solidus temperatures for the candidate materials are different, various heat energy inputs were needed to melt the metal powder in LMD, in order to keep the shape of the thin wall uniform and rectangular.

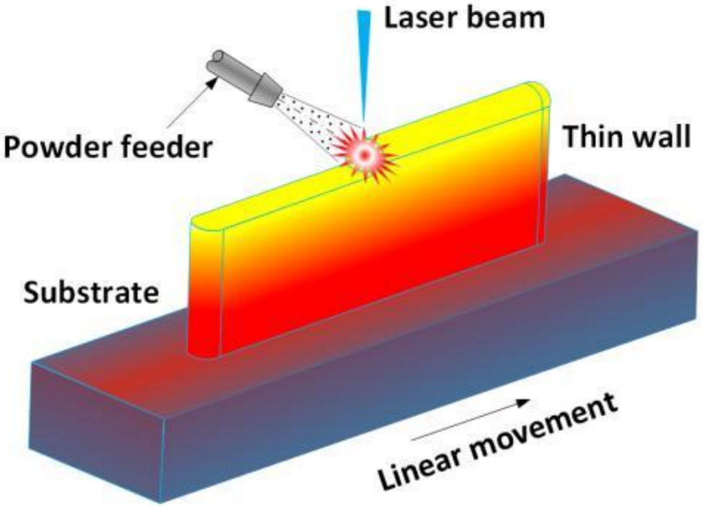

Figure 3.4. LMD thin wall sample.

Table 3.3. The laser processing parameters in LMD

Parameter	Value			
	V	Cr	Fe	SS316
Output power (W)	1000	1000	700	550
Beam diameter (mm)	2			
Scan speed (mm/min)	200			
Shielding gas	Argon			
Powder feed rate (g/min)	5.1	6.3	7.6	7.2

4. RESULTS AND DISCUSSION

4.1. EDS AND SEM ANALYSIS

4.1.1. Specimen Preparation. A specimen was cut off of the thin wall sample using the Hansvedt Electric Discharge Machine (EDM). The specimen was then mounted on mounting pressure equipment (Simplimet 1000) using a phenolic resin powder. Then, the offcut cutting surface was grinded using abrasive papers from 180 Silicon Carbide Grit to 1200 Silicon Carbide Grit. After that, the specimen was polished using colloidal silica with a median particle size of 0.05 µm. The final prepared specimen is shown in Figure. 4.1.

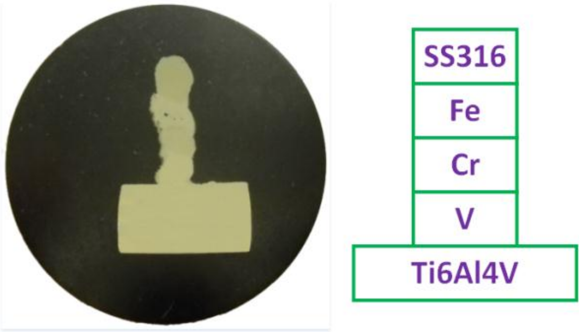

Figure 4.1. The final prepared specimen.

4.1.2. EDS Point Test and SEM Test Results. The intended transition of Ti6Al4V to SS316 was deposited by starting with a Ti6Al4V substrate with V as the first layer, then Cr, Fe, and SS316 as the final deposit. EDS point test and SEM test were carried out from Ti6Al4V substrate to SS316, to observe the solidification microstructure and composition distribution along the composition route.

EDS was used to analyze the element concentration distribution along the transition composition route. The analyses were performed on Helios NanoLab 600 coupled with an Oxford EDS extension. 115 sample points uniformly distributed along the route. The bottom of first point is aligned with surface of substrate. The interval between two adjacent points is 0.1 mm. Dwell time for each point is 5s. All the EDS point test data for composition curves was plot in Figure.4.2. The element distribution curves along the transition composition route on the specimen surface show some interesting features such as intersection, immediate lift and dip, and stagger up and down. These kinds of phenomenon can demonstrate the clear element concentration tendency along the transition composition. Three ridges indicate three transition metals: V, Cr, Fe. V and Cr can diffuse to other metal layers easily. Element diffusion is obvious due to multiple heating and high temperature gradient in LMD.

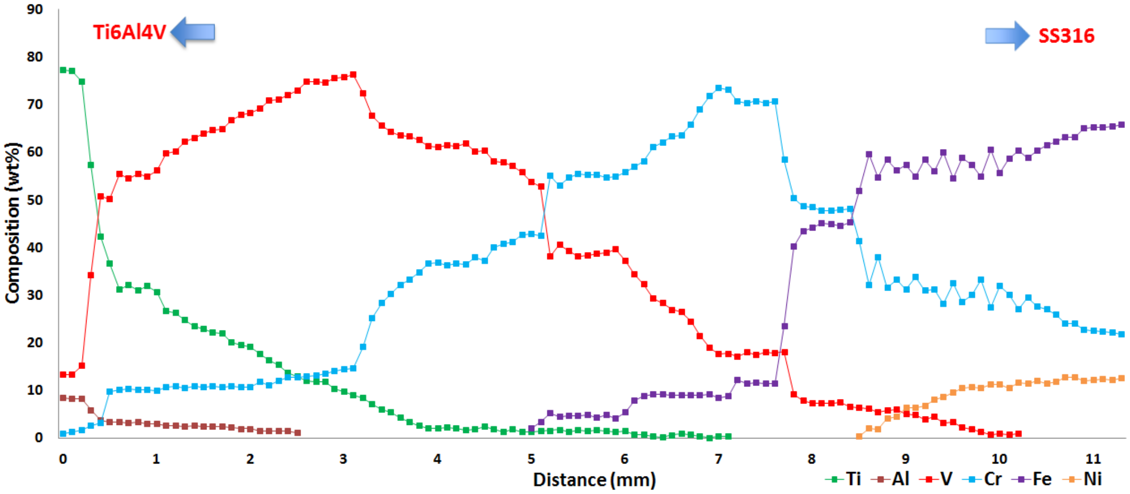

Figure 4.2. The EDS point test result for composition curve.

To observe the microstructure, four sample sites were selected along the route, whose positions were determined by the maximum weight percentage of Ti, V, Cr, Fe based on the EDS point test in Figure 4.3. SEM tests were done on the four selected sites. Figure 4.3 shows the microscopic images of microstructure at the four sample sites.

Figure 4.3(a) depicts the microstructure close to the Ti6Al4V substrate, where Ti concentration is highest. It is clear to observe the interface between substrate and V layer. On the left side of interface, the Ti6Al4V region exhibits an elongated lamellar-type microstructure. This is expected because the substrate surface is completely melted and re-solidified during LMD process and undergoes rapid solidification. High cooling rate causes this type of microstructure. Closer to the interface, thinner and smaller of the microstructure is. From the interface to the Ti6Al4V, it is clear to find the grain's epitaxial growth in solidification. On the right side of interface, close to V region, some pores are observed which formed in the LMD process. Figure 4.3(b) depicts the microstructure with maximum V concentration. The microscopic image exhibits an equiaxed microstructure. Due to the high cooling rate in rapid solidification, the equiaxed microstructure is elongated approximately along the cooling direction. It can be noticed that gas porosity occurred in V layer. Figure 4.3(c) depicts the microstructure in the region with highest Cr con-centration. An equiaxed-type microstructure is observed in this region. Rapid solidification results in the elongated microstructure. Gas porosity is again found in the Cr-rich layer. Figure 4.3(d) depicts the microstructure where Fe concentration is highest. In this region the microstructure exhibits a classic ferrite equiaxed grain. Some tiny gas pores can be found in some area.

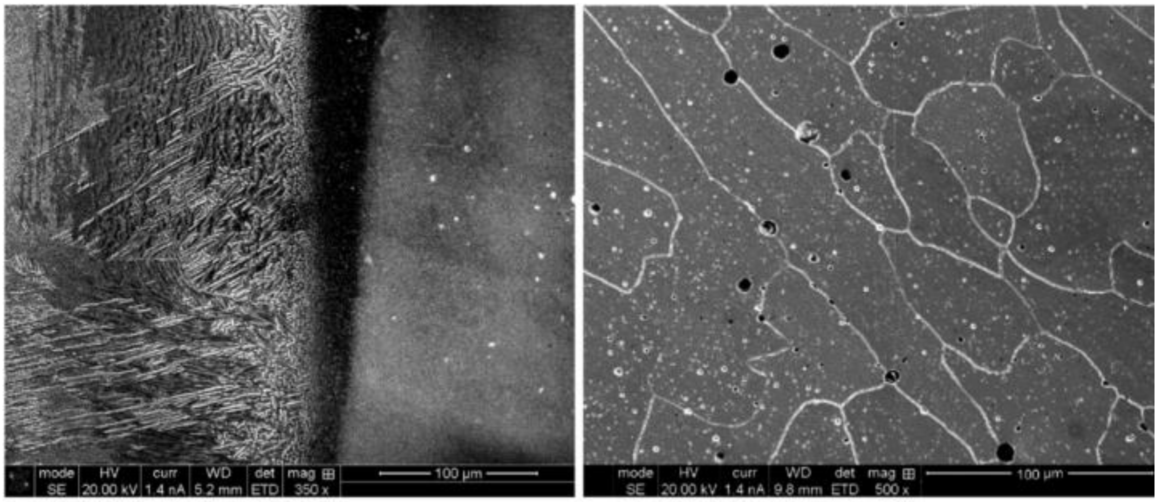

(a) (b)

Figure 4.3. The microscopic images of microstructure at the four sample sites.

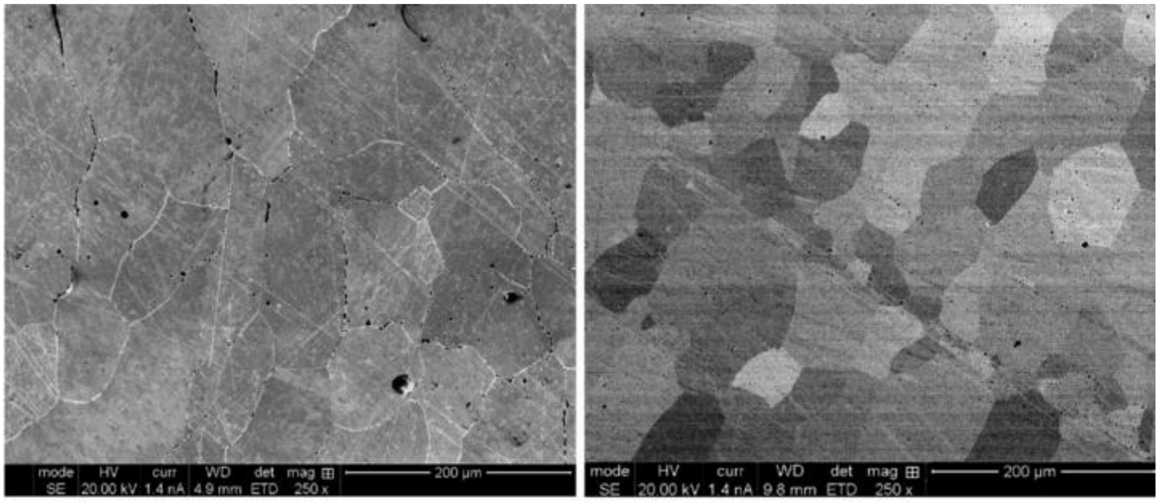

(c) (d)

Figure 4.3. The microscopic images of microstructure at the four sample sites (cont.).

4.1.3. XRD Analysis. XRD tests were used to identify the phases on each site. The XRD tests were operated with XPERT Pro-type diffractometer. The anode material was Cu. All the XRD patterns on four sites, determined by the maxi-mum weight percentage of Ti, V, Cr, Fe, are shown in Figure 4.4. An obvious tendency can be found. These four XRD patterns can indicate the gradual transition from Ti6Al4V to SS316.

On the first site, dot is used to represent α-Ti. Diamond indicates β-Ti. Inverted triangle indicates Ti3Al. All of them are the primary phases in Ti6Al4V. In addition, (V, Cr) solid solution has strong intensity. Another β-Ti with bcc structure can be detected. It is the solid solution between Ti and Cr. Multiple heating and high temperature gradient in LMD cause Cr diffuse in V layer and even near Ti6Al4V. Diffused Cr forms into solid solution with V and Ti respectively. Some bcc peaks are lost in XRD pattern. It is mainly caused by preferred orientation or texture. When the specimen is prepared for XRD test, grinding and polishing may cause the multi crystal's grain directions to be oriented. The XRD pattern on site-2 is similar with site-1. The intensity of α-Ti and β-Ti is weakening, but still obvious. The intensity of (V, Cr) is stronger than site-1. The reason should be the higher concentrations of Cr and V on site-2. On the site-3, the α-Ti and β-Ti are not detected. The intensities of (αFe, V) and (αFe, Cr) keep increasing. (αFe, V) is bcc solid solution of Fe and diffused V. (αFe, Cr) is the solid solution of Fe and Cr, which is also called ferrite with bcc structure. Austenitic fcc solid solution (γFe, Ni) is detected. This austenite phase may be in SS316 layer, just detected by larger XRD sample ar-ea. There are two kinds of Fe-Cr solid solutions α and α’. The (α’Fe, Cr) is high concentration Cr bcc, while (αFe, Cr) is low concentration Cr bcc. Both of them precipitate from the segregation of ferritic solid solution α(δ). In the XRD pattern on site-4, the ferrite bcc has strong intensity. Austenite (γFe, Ni) fcc can also be detected. The XRD pattern on site-4 is close to SS316.

From site-1 to site-3, α-Ti and β-Ti decrease and disappear. On the other hand, ferrite and austenite start to appear from site-3, and increase to the major phases on site-4. Since V, Cr and Fe are added as intermediate metal, some solid solutions are detected in the transition layers. The XRD patterns can verify the material transition design from Ti6Al4V to SS316. In addition, the XRD patterns on the four sites indicate that there is not intermetallic phase. Therefore, XRD analysis can demonstrate the intermetallic phases are effectively eliminated using the transition composition route with design in Figure 3.2.

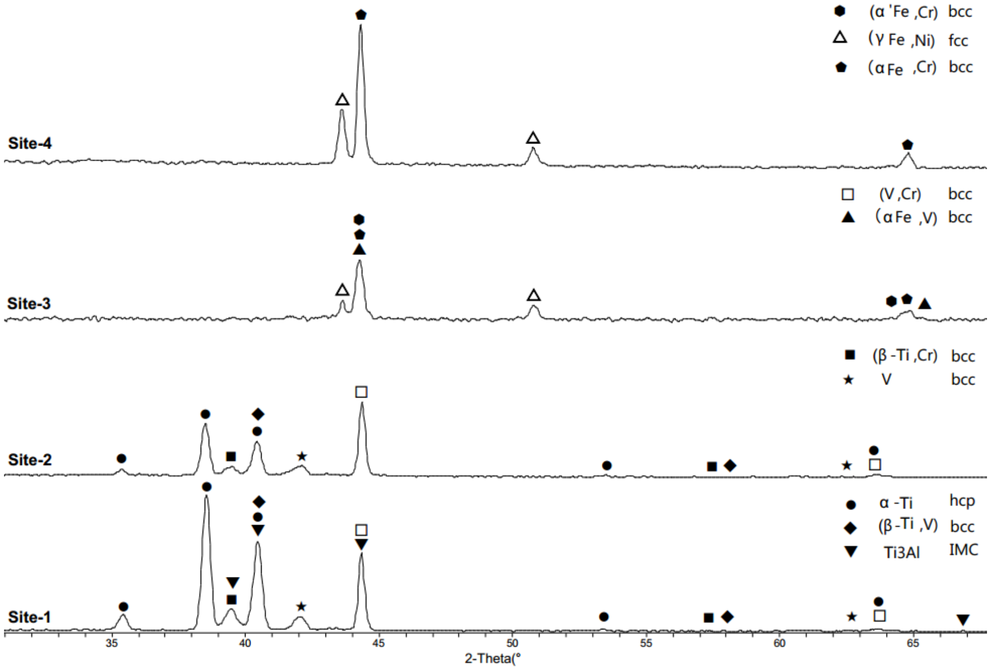

Figure 4.4. XRD patterns in the four observation sites.

4.1.4. Vickers Hardness Analysis. Generally, hardness is an important material property that can indicate the resistance to plastic deformation by penetration. The Vickers hardness test applies an inverted diamond pyramid as an indenter. It is adapted for micro hardness testing for various materials such as metals, alloys, ceramics, composites, etc. For this research, one reality is that the micro hardness of the intermetallic phase is far greater than the pure metal and alloy in the composition route. Therefore, the Vickers hardness test is useful to locate the possible formation of the intermetallic phase.

The thin wall sample was cut transversely by the wire electrical discharge machine (Hansvedt DS-2 Traveling Wire EDM) to acquire the cross section. Thirty Vickers hardness sampling points were distributed along the composition route to cover all the candidate materials. The cut sample was pressed into the mounting material in order to fit the Vickers hardness tester conveniently. The sample preparation is shown in Figure 4.1. The Vickers hardness test was performed at room temperature using a Struers Duramin-5 hardness tester with a press load of 9.81 N and load time of 10 s. Indentions started at the SS316 edge and continued at various spacing into the Ti6Al4V substrate region.

Figure 4.5 shows the Vickers hardness test values along with indications of what material region these values belong to. The hardness values were stabilized throughout the SS316 region at 281±19 HV. The highest hardness values were observed around the Fe-Cr interface followed by a slight decrease in hardness value at the Cr-V interface, and then a slight increase in hardness value at the Fe-V interface. The subsequent increase in the Ti6Al4V region was stabilized at 375 ±16 HV. In the total Vickers hardness number (VHN) distribution, the maximum hardness value was 425.3 HV. There is no obvious volume of high VHN areas in the distribution. All the VHN gradients were slight instead of steep changes. When compared to the result in Figure 2.3, the Vickers hardness test result on the sample reveals that there is no significant formation of intermetallic phase if the transition composition route is utilized.

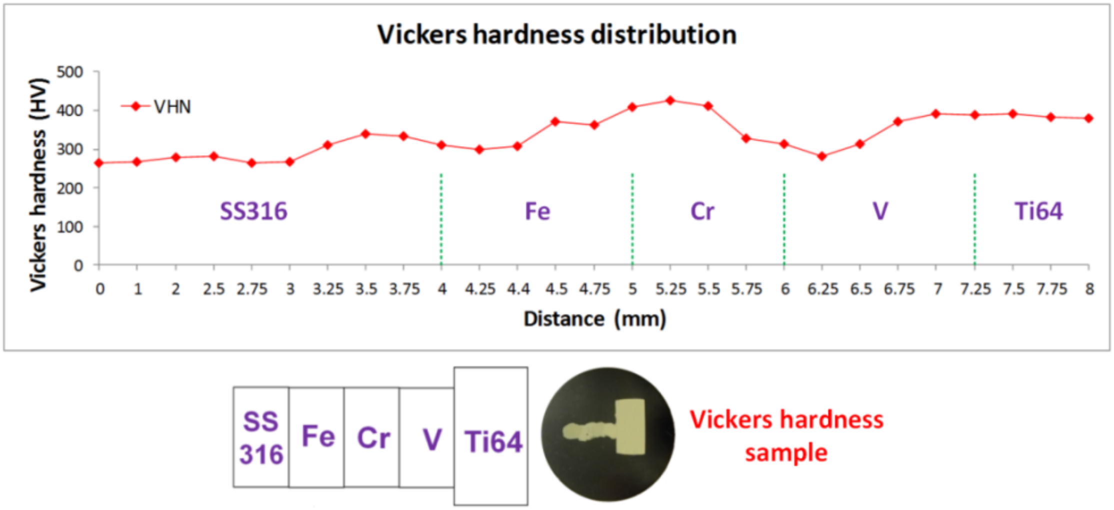

Figure 4.5. The sample preparation and Vickers hardness result.

5. CONCLUSION

By the process of LMD, Ti-Fe intermetallic phases formed in directly depositing SS316 powder on Ti6Al4V are investigated. Then the intended filler materials design from Ti6Al4V to SS316 was deposited by starting with a Ti6Al4V substrate with V as the first layer of deposit, then Cr, Fe, and SS316 as the final layer. Based on the above analysis, some conclusions are generalized as follows:

- ✧ In the process of LMD, the stainless steel layer directly fell off from titanium substrate coupled with clear cracking sound. By observing this fracture morphology, the fracture mechanism is classic cleavage fracture. This indicates that the formed phase in fracture area is very hard and brittle, and almost without any plasticity. The XRD pattern in the fracture area indicates main intermetallic phases are Fe2Ti and FeTi. The brittleness and hardness of these two caused the direct fracture and clear cracking sound under thermal stress and excessive generation of strains at the interface of titanium and stainless steel alloys. The VHN near fracture is much larger than the base alloys on both sides. The VHN distribution illustrates that intermetallic phases is the primary cause for the failure.
- ✧ A new transition route: Ti6Al4V→V→Cr→Fe→SS316, is explored to effectively eliminate the formation of Ti-Fe intermetallics. With this route, a functionally graded material between Titanium alloy and stainless steel is fabricated by LMD. The element distribution curves show some interesting features such as intersection, immediate lift and dip, and stagger up and down. These kinds of phenomenon can demonstrate the clear element concentration gradient along the transition composition. The SEM images indicate rapid solidification and high cooling rate result in the elongated microstructure. The XRD patterns show that pure metals are hard to find. Most of them exist in form of stable solid solution. Multiple heating and high temperature gradient in LMD cause the diffusions. There is not intermetallic phase detected on the four test sites. Therefore, the transition composition route design can be used to effectively eliminate the Ti-based intermetallic phases between Ti6Al4V and SS316 alloys. This conclusion

can also be verified by the Vickers hardness test results. In the total VHN distribution, there is no obvious volume of high VHN areas. All the VHN gradients were slight instead of steep changes.

BIBLIOGRAPHY

[1] Lee M, Park J, Lee J and Rhee C. Phase-dependent corrosion of titanium-to-stainless steel joints brazed by Ag–Cu eutectic alloy filler and Ag interlayer. Journal of Nuclear Materials 2013; 439: 168-173.

[2] Li P, Li J, Xiong J, Zhang F and Raza SH. Diffusion bonding titanium to stainless steel using Nb/Cu/Ni multi-interlayer. Materials Characterization 2012; 68: 82-87.

[3] Atasoy E and Kahraman N. Diffusion bonding of commercially pure titanium to low carbon steel using a silver interlayer. Materials Characterization 2008; 59: 1481-1490.

[4] Ting W, Zhang B-G, Chen G-Q, Feng J-C and Qi T. Electron beam welding of Ti-15-3 titanium alloy to 304 stainless steel with copper interlayer sheet. Transactions of Nonferrous Metals Society of China 2010; 20: 1829-1834.

[5] Elrefaey A and Tillmann W. Solid state diffusion bonding of titanium to steel using a copper base alloy as interlayer. Journal of Materials Processing Technology 2009; 209: 2746-2752.

[6] Kundu S, Sam S and Chatterjee S. Interfacial reactions and strength properties in dissimilar titanium alloy/Ni alloy/microduplex stainless steel diffusion bonded joints. Materials Science and Engineering: A 2013; 560: 288-295.

[7] Kundu S and Chatterjee S. Interface microstructure and strength properties of diffusion bonded joints of titanium–Al interlayer–18Cr–8Ni stainless steel. Materials Science and Engineering: A 2010; 527: 2714-2719.

[8] Lee M, Lee J, Choi Y, Kim D, Rhee C, Lee Y and Hong S. Interlayer engineering for dissimilar bonding of titanium to stainless steel. Materials letters 2010; 64: 1105-1108.

[9] ZHANG B-g, Ting W, DUAN X-h, CHEN G-q and FENG J-c. Temperature and stress fields in electron beam welded Ti-15-3 alloy to 304 stainless steel joint with copper interlayer sheet. Transactions of Nonferrous Metals Society of China 2012; 22: 398-403.

[10] Sieurin H and Sandström R. Sigma phase precipitation in duplex stainless steel 2205. Materials Science and Engineering: A 2007; 444: 271-276.

[11] Michalska J and Sozańska M. Qualitative and quantitative analysis of σ and χ phases in 2205 duplex stainless steel. Materials Characterization 2006; 56: 355-362.

[12] Hsieh C-C and Wu W. Overview of Intermetallic Sigma (ISRN Metallurgy 2012; 2012:

[13] Murray JL. Phase diagrams of binary titanium alloys. ASM International, 1987 1987; 354.

[14] Chan KW and Tjong SC. Effect of secondary phase precipitation on the corrosion behavior of duplex stainless steels. Materials 2014; 7: 5268-5304.

[15] Amine T, Newkirk JW and Liou F. An investigation of the effect of direct metal deposition parameters on the characteristics of the deposited layers. Case Studies in Thermal Engineering 2014; 3: 21-34.

VITA

Wei Li was born in Baotou, Inner Mongolia, China. He received his Bachelor degree in the major of mechanical design manufacturing and automation from University of Electronic Science and Technology of China (UESTC) in 2005. Then he worked as Manufacturing engineer in Aerospace Science and Technology Cooperation in China from 2005 to 2009. He received his Master degree in Engineering Mechanics from Tongji University in 2012. After that, he joined Missouri University of Science and Technology to start the 2nd Master program. During his graduate studies he held the position Graduate Research Assistant in the Laser Aided Manufacturing Process Laboratory. He received his Master of Science degree in Manufacturing Engineering from Missouri University of Science and Technology, Rolla, Missouri, USA in July 2017.